







The antiferromagnetic phase transition in the layered $\text{Cu}_{0.15}\text{Fe}_{0.85}\text{PS}_3$ semiconductor: experiment and DFT modelling

V. Pashchenko ¹, O. Bludov ¹, D. Baltrunas ², K. Mazeika ², S. Motria³, K. Glukhov ^{3*}, Yu. Vysochanskii ³.

¹ B. Verkin Institute for Low Temperature Physics and Engineering of NAS of Ukraine, 47 Nauky Ave., 61103, Kharkiv, Ukraine

² Department of Nuclear Research Center for Physical Sciences and Technology, 231 Savanoriu ave., LT-02300, Vilnius, Lithuania

³ Institute for Solid State Physics and Chemistry, Uzhhorod National University, 54 Voloshyn Str., 88000, Uzhhorod, Ukraine

Received July 23, 2022, in final form October 15, 2022

The experimental studies of the paramagnetic-antiferromagnetic phase transition through Mössbauer spectroscopy and measurements of temperature and field dependencies of magnetic susceptibility in the layered $\text{Cu}_{0.15}\text{Fe}_{0.85}\text{PS}_3$ crystal are presented. The peculiar behavior of the magnetization — field dependence at low-temperature region gives evidence of a weak ferromagnetism in the studied alloy. By the ab initio simulation of electronic and spin subsystems, in the framework of electron density functional theory, the peculiarities of spin ordering at low temperature as well as changes in interatomic interactions in the vicinity of the Cu substitutional atoms are analyzed. The calculated components of the electric field gradient tensor and asymmetry parameter for Fe ions are close to the ones found from Mössbauer spectra values. The Mulliken populations show that the main contribution to the ferromagnetic spin density is originated from $3d$ -copper and $3p$ -sulfur orbitals. The estimated total magnetic moment of the unit cell (8.543 emu/mol) is in reasonable agreement with the measured experimental value of ~ 9 emu/mol.

Key words: metal phosphorus trichalcogenides, magnetic ordering, Mössbauer spectroscopy, phase transition, density functional theory

1. Introduction

Two-dimensional (2D) van der Waals (vdW) materials offer possibilities to study novel physical properties and explore their potential applications in electronic, optical, and spintronic devices in the nanoscale [1]. The realization of magnetism in easily exfoliated layered crystals provides accessibility to control and manipulate magnetic properties at a single atomic layer level [2–6]. The presence of multiferroicity in such materials, when they exhibit two or more primary ferroic properties, is important for potential applications in the non-volatile storage devices controlled by an external electric field.

Recently, 2D ferroelectric polarization was found in CuInP_2S_6 several layers flakes and even in monolayers [7, 8]. On the other hand, 2D antiferromagnetism is also demonstrated for CuCrP_2S_6 layers [9]. Furthermore, multiferroic material can be prepared by doping or modifying some monolayers, such as black phosphorus and graphene [10]. 2D materials with spontaneous ferromagnetism and ferroelectricity have rarely been reported. Recently, it was found that 2D CuCrP_2S_6 is multiferroic with magnetism and ferroelectricity stems from Cr and Cu cations, and the magnetoelectric coupling follows from

*Corresponding author: kglukhov@gmail.com

the spin-orbit interaction [11]. Copper chromium thiophosphate CuCrP_2S_6 is an antiferromagnetic-antiferroelectric multiferroic involving collective ordering mechanisms of magnetic Cr^{3+} ions and off-centered Cu^+ ions, respectively [12]. The indium compound CuInP_2S_6 belongs to the same $C2/c$ space group as CuCrP_2S_6 at room temperature, but due to a specific second-order Jahn–Teller instability of Cu^+ , it attains a ferroelectric structure with Cc symmetry below $T_c \approx 315$ K. The solid solutions $\text{CuCr}_{1-x}\text{In}_x\text{P}_2\text{S}_6$ reveal disordered dipolar glass phases, because of randomness and frustration, and quasimolecular magnetic properties [13]. Dynamic polar clustering occurs in these solid solutions and superposes structural glassiness to the ferroelectric long-range Cu^+ order at low temperatures.

Transition metal phosphorus trichalcogenides MPS_3 ($M = \text{Mn, Fe, Co, Ni, \dots}$) have monoclinic crystal structure (space group of $C2/m$), in which the metal cations (M) are surrounded by an octahedral cage of $(\text{P}_2\text{S}_6)^{4-}$ bipyramids, and the neighboring metals have a 2D honeycomb lattice arrangement [5]. The crystal layers stack with vdW forces. Resulting from the competitions between the direct M – M exchange and indirect superexchange, mediated through S^{2-} anions within each layer, as well as the interlayer exchange, determine antiferromagnetic (AFM) ordering temperature T_N and its type — zigzag, Neel or stripy pattern [14].

In 2D materials, magnetic anisotropy is also crucial in establishing a long-range correlation. For FePS_3 compound, the trigonal distortion combined with the spin-orbit coupling yields a large single-axis magnetic anisotropy [15], and it can be described by the Ising model. In this compound, the long-range order is present in the direction perpendicular to the crystal layers, and FePS_3 has a zigzag type of antiferromagnetic ground state.

Incorporation of atomic defects and chemical substitutions in MPS_3 2D materials could manipulate and control their magnetic properties [16–18]. Distinct magnetic order, spin direction, and magnetic anisotropy, exotic phases and properties are expected to be revealed in solid solutions of these layered crystals. For example, spin glass behavior was found in $\text{Fe}_{1-x}\text{Mn}_x\text{PS}_3$ [19, 20] and in $\text{CuCr}_{1-x}\text{In}_x\text{P}_2\text{S}_6$ [13].

In this paper there are presented magnetic properties of FePS_3 as a function of temperature, field and dilution of the magnetic atoms by means of substitution of a non-magnetic species, in this case copper — we studied the magnetic properties of 2D vdW layered $\text{Cu}_{0.15}\text{Fe}_{1.85}\text{PS}_3$. The crystalline flakes with stoichiometry $\text{Cu}_{0.15}\text{Fe}_{1.85}\text{PS}_3$ were grown using the gas transport method [21]. By dielectric, specific heat, and ultrasonic measurements the structural phase transition close to 109 K was found in these crystals [21]. Obviously, similarly to FePS_3 , it should be the antiferromagnetic phase transition. In this work, using the Mössbauer spectroscopy and magnetic investigations, together with first-principles studies, the peculiarities of magnetic ordering in the $\text{Cu}_{0.15}\text{Fe}_{1.85}\text{PS}_3$ alloy are traced with the aim to search for a new layered multiferroic material for nanoscale devices.

2. Mössbauer data

Mössbauer spectra were measured using $^{57}\text{Co}(\text{Rh})$ source in the transmission geometry. The sample was composed of not grinded separate plates. The low-temperature spectra were obtained using the closed cycle He cryostat (Advanced Research Systems, Inc.). The doublet and Hamiltonian were applied to fit the Mössbauer spectra using WinNormos Site software [22]. Isomer shift is presented relative to α -Fe at room temperature.

Mössbauer spectra displays the transition from an antiferromagnetic state to a paramagnetic state near the 110 K temperature (figure 1). Above the antiferromagnetic transition temperature, Mössbauer spectra were fitted to one doublet. On contrary, the magnetic subspectra (Hamiltonian method in Normos Site) should be used to fit the Mössbauer spectra below the transition temperature. Previously, the spectra of FePS_3 were fitted using one set of hyperfine parameters (one subspectrum) [23]. We found that for $\text{Cu}_{0.15}\text{Fe}_{1.85}\text{PS}_3$, a good quality of fitting was achieved using three subspectra described by Hamiltonian method (WinNormos Site) in the case of single crystal [24] except the spectra measured above 103 K temperature and below transition point which were broadened and needed extra subspectra to fit. These spectra were fitted using hyperfine field distribution. The set of Hamiltonian parameters included electric field gradient (EFG) asymmetry parameter η and angles θ and β . θ is the angle between z axis of EFG system and the direction of the magnetic field while β is between z axis of EFG system and γ -ray direction. The isomer shift δ and quadrupole coupling constant $eQV_{zz}/2$, where Q is nuclear quadrupole

moment, V_{zz} is EFG tensor component, were the same for all three subspectra. The main area (70–75%) of the Mössbauer spectrum below 102 K can be attributed to two magnetically split subspectra having hyperfine fields B_1 and B_2 differing approximately by 1T (figure 2 a). However, the effective hyperfine field of them (B_{12}) was very close to that found for FePS_3 [23, 25]. For these two subspectra, θ and β angles were fixed to zero i.e., $\theta = 0$ and $\beta = 0$. In this case, z axis of EFG and the magnetization were normal to ab -plane similar to single-crystalline FePS_3 . For both subspectra, the combined quadruple and magnetic interactions gave two sets of overlapping four lines (figure 1). For the third subspectrum fitted to the experimental spectra, the angles were allowed to change and the best fits were obtained for $\theta \approx 10\text{--}30^\circ$ and $\beta \approx 20\text{--}40^\circ$. Moreover, the asymmetry parameter $\eta \approx 0.76$ for the third subspectrum was larger than that of the first two subspectra ($\eta = 0.23\text{--}0.28$). Therefore, taking the Cu atoms distribution into consideration, the third subspectrum can be considered to be due to distorted iron atom sites having Cu atoms as first neighbours in hexagonal arrangement of metal atoms along ab -plane. Thus, the other two subspectra were attributed to iron sites similar to FePS_3 [23, 25]. It should be noted that FePS_3 undergoes first order phase transition at 120 K temperature. Coexistence of paramagnetic and antiferromagnetic phases was observed [23]. For $\text{Cu}_{0.15}\text{Fe}_{0.85}\text{PS}_3$, the paramagnetic doublet starts also appear together with much more broadened magnetically split part of spectra above 102 K.

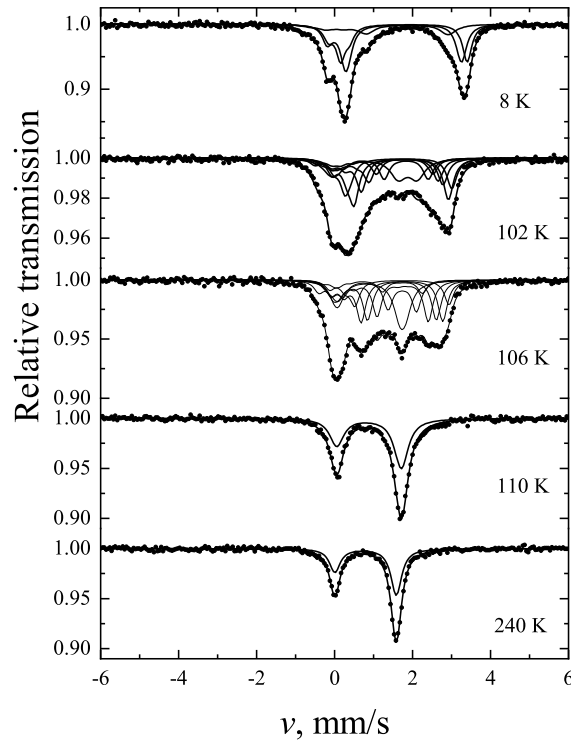


Figure 1. Mössbauer spectra of $\text{Cu}_{0.15}\text{Fe}_{0.85}\text{PS}_3$ measured at the indicated temperature.

The lines of the doublet can be attributed to γ -ray transitions to $\pm 3/2$ and $\pm 1/2$ excited energy levels of ^{57}Fe nucleus. The line intensity ratio of 1.8–2.03 found above the phase transition temperature (figure 2 d) according to

$$I_{3/4}/I_{1/2} = (1 + \cos^2 \beta)/(5/3 - \cos^2 \beta)$$

gave the angle $\beta = 27\text{--}32^\circ$. Here, it is assumed that the EFG asymmetry parameter $\eta = 0$. Quadruple splitting $\Delta = (eQV_{zz}/2) (1 + \eta^2/3)^{1/2}$ was somewhat different below and above the antiferromagnetic

transition point. This can be explained by the first-order transition because the lattice undergoes some transformations [23], as in the case of FePS₃ when $V_{zz} > 0$.

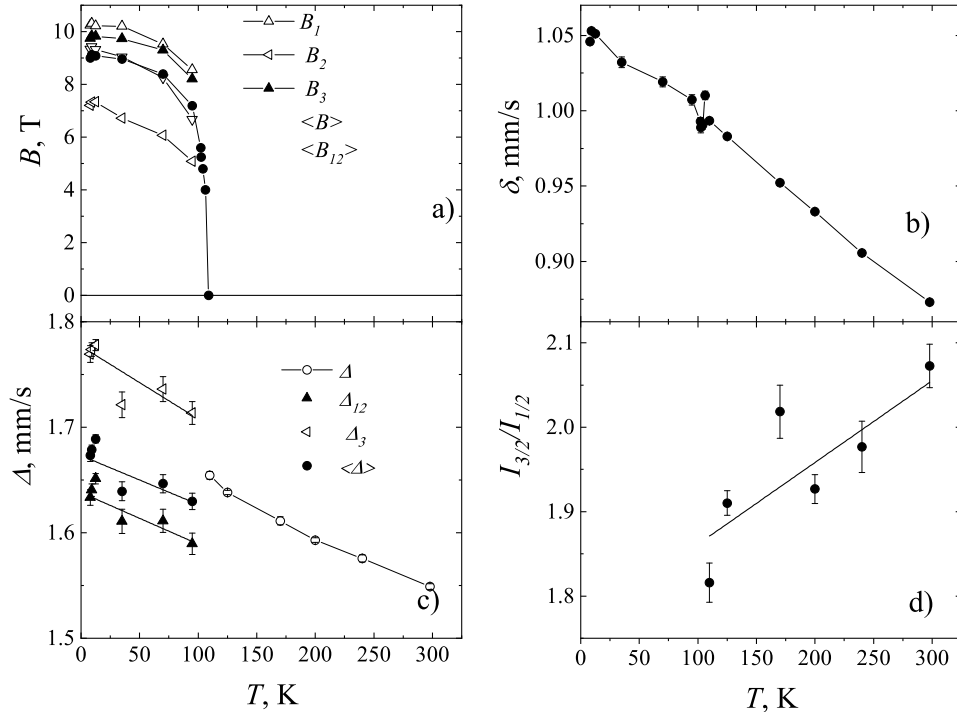


Figure 2. Dependence of hyperfine field B (a), isomer shift δ (b), quadrupole splitting Δ (c) and intensity ratio of lines of doublet (d) of Mössbauer spectra of $\text{Cu}_{0.15}\text{Fe}_{0.85}\text{PS}_3$ crystal on temperature.

3. Magnetic moment measurements

3.1. Temperature dependence of the magnetic susceptibility

Single crystal $\text{Cu}_{0.15}\text{Fe}_{0.85}\text{PS}_3$ sample, of $\sim 3 \times 4$ mm flake-shaped (depicted in figure 3) and 1.54 mg was used for magnetic moment measurements. For all orientations of the external magnetic field at a temperature of about 108 K, a sharp change in the temperature dependence of the magnetic susceptibility (see figure 4) was observed, which may indicate the presence of a magnetic phase transition at this temperature.

No narrow anomaly associated with 3D ordering is observed on the $\chi(T)$ curve in the region of 108 K. Therefore, it is possible that the ordering can also occur at a higher temperature, and in this case, we are dealing with a phase transformation of a magnetically ordered phase. For $H \perp$ plane of crystal layers and $T < 108$ K, as the temperature is lowered, the magnetic susceptibility $\chi(T)$ of the sample decreases significantly, which is typical when antiferromagnetic correlations are established in the spin system.

In addition to the experimental curves $\chi(T)$ (in a constant magnetic field $H = 2000$ Oe) in figure 4, the asterisks show several estimates of the values of the magnetic susceptibility of the $\text{Cu}_{0.15}\text{Fe}_{0.85}\text{PS}_3$ sample obtained by analyzing the linear sections of the field dependence $M(H)$ measured up to 5 T [see $M(H)$ in the following figures]. As seen in figure 4, the match for the orientation of the $H \parallel$ plane

is perfect, with little deviation found between different experimental techniques for the $H \perp$ plane. The latter seems to be connected with the discovery of remanent magnetization (or a spontaneous weakly ferromagnetic moment in an antiferromagnet as a result of a small sublattice canting) in experiments for the $H \perp$ plane.

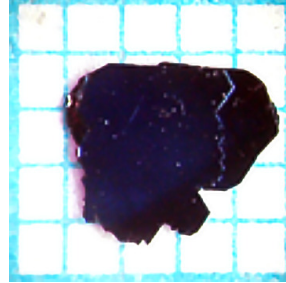


Figure 3. (Colour online) The sample of $\text{Cu}_{0.15}\text{Fe}_{0.85}\text{PS}_3$ crystal used for magnetic moment measurements.

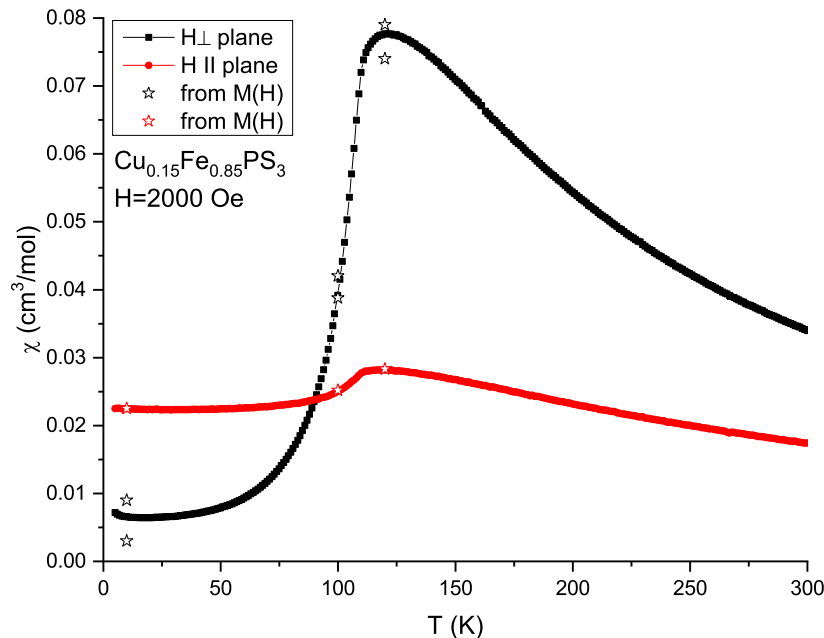


Figure 4. (Colour online) Temperature dependence of the magnetic susceptibility $\chi(T) = M(T)/H$ of a $\text{Cu}_{0.15}\text{Fe}_{0.85}\text{PS}_3$ single crystal in magnetic field $H = 2000$ Oe for two directions $H \perp$ plane and $H \parallel$ plane of crystal layers.

3.2. Field dependence of the magnetic moment

The field dependencies of the magnetic moment of the $\text{Cu}_{0.15}\text{Fe}_{0.85}\text{PS}_3$ sample were studied at 120 K — above the assumed phase transition, 100 K — approximately the middle of the phase transformation, and 10 K — the low-temperature point, where all the magnetic transformation processes have already been completed based on their general form $\chi(T)$. All the obtained curves $M(H)$ for the $H \perp$ plane and $H \parallel$ plane of crystal layers are shown in figure 5. All of them demonstrate a fairly good linear behavior of $M(H)$ at any temperatures both above and below the assumed phase transition.

For the $H \perp$ plane at $T = 10$ K, extrapolation of the linear dependence (region above 2000 Oe) to zero magnetic fields detects the presence of a non-zero residual magnetic moment of the sample of the

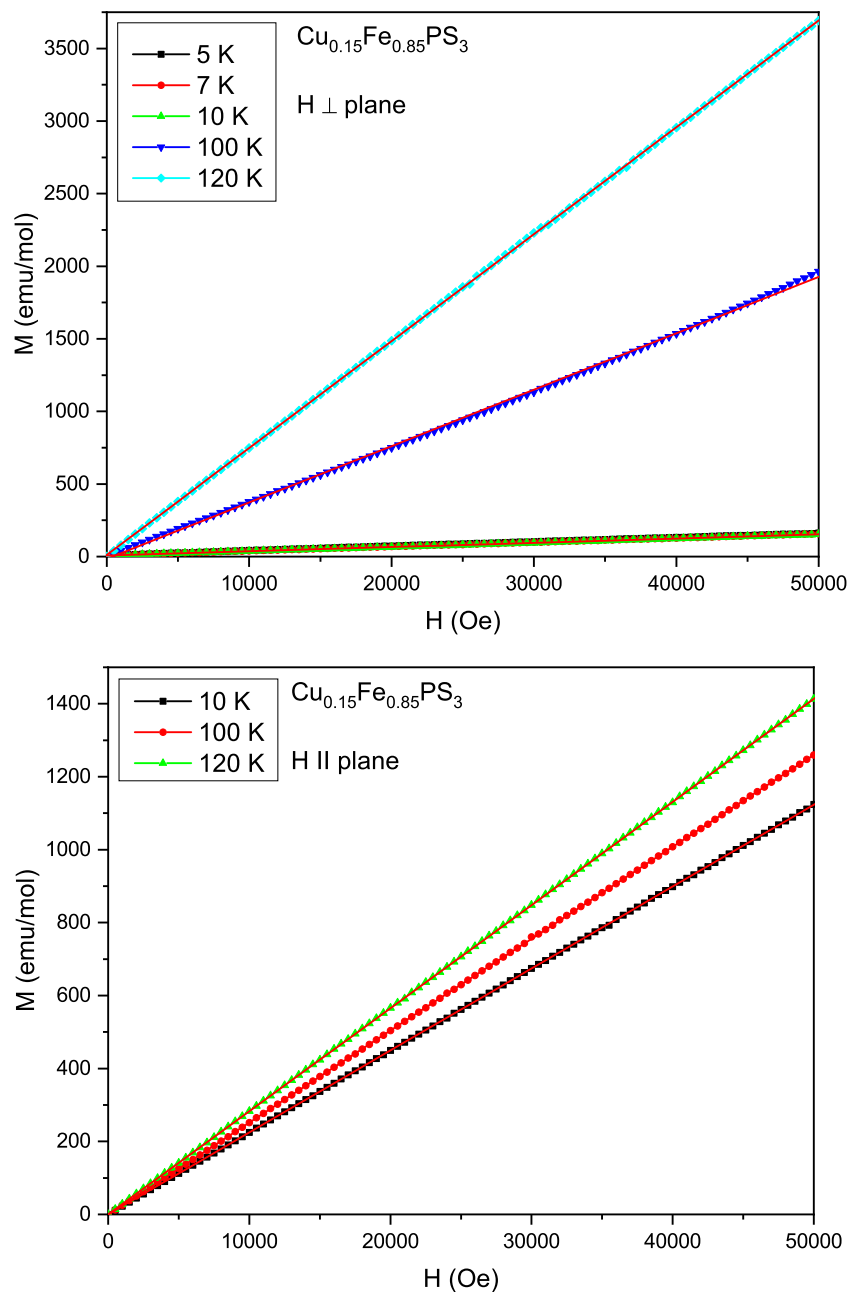


Figure 5. (Colour online) Field dependence of the magnetic moment $M(H)$ of $\text{Cu}_{0.15}\text{Fe}_{0.85}\text{PS}_3$ sample at different temperatures for two orientations of the magnetic field: $H \perp$ plane (top panel) and $H \parallel$ plane of crystal layers (bottom panel).

order of 9 emu/mol (dotted line in the insertion in figure 6). This may be due to the existence of a canted magnetic sublattice in an ordered antiferromagnetic system and, hence, to a weak ferromagnetic moment of the system in this direction. At the same time, such a feature in $M(H)$ is completely absent for the other direction of the $H \parallel$ plane. This behavior of the magnetization for the $H \perp$ plane can be satisfactorily explained within the framework of the four-sublattice model of an antiferromagnet of the flat cross-type. In very weak fields, the ground state will be similar to the state with latent ferromagnetism and the total moment of the system will be close to zero. A rapid increase in the magnetization with the increasing field

will occur due to the orientational flip of a skewed pair with a weakly ferromagnetic moment oriented against the field to the direction of the skewed pair in which this moment is oriented along the field. In the fields above 2000 Oe, the four-sublattice system effectively turns into a simple two-sublattice system, in which the brace between the sublattices gives a weak moment along the field.

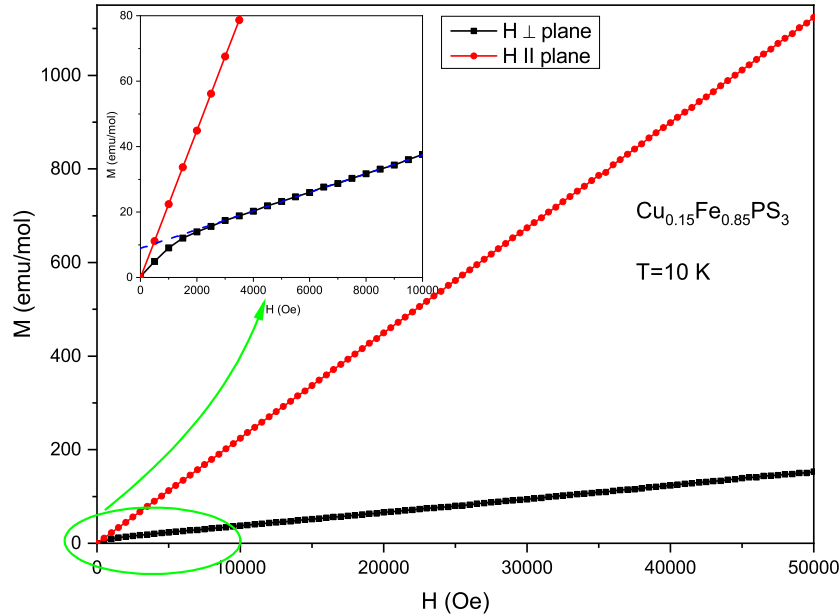


Figure 6. (Colour online) Field dependence of the magnetic moment of the $\text{Cu}_{0.15}\text{Fe}_{0.85}\text{PS}_3$ sample at a temperature of $T = 10$ K for $H \perp$ plane and $H \parallel$ plane. The insertion shows a low-field region.

Thus, a characteristic field of about 2000 Oe can be considered as a phase transition field between the effective four-sublattice and two-sublattice magnetic structures for the system under study.

4. *Ab initio* simulation results

The QUANTUM ESPRESSO package [26], was used to perform calculations. They were carried out within the generalized gradient approximation (GGA) with the Perdew–Burke–Ernzerhof functional [27] or with the CA-PZ local functional based on the Ceperley and Alder data [28] parameterized by Perdew and Zunger [29]. The layered $\text{Cu}_{0.15}\text{Fe}_{0.85}\text{PS}_3$ crystal possesses the so-called vdW gap between layers. Therefore, the DFT-D method taking into account the dispersion interaction elaborated by Grimme [30] is needed to calculate electronic properties of the material. The ultra-soft pseudopotential [31] was used to perform calculations for Fe — $3d^6 4s^2$, Cu — $3d^{10} 4s^1$, P — $3s^2 3p^3$, S — $3s^2 3p^4$ atomic configurations. The plane-wave basis set cut-off was chosen to be equal to 600 eV. The Monkhorst–Pack k -points grid [32] sampling was set at $12 \times 12 \times 3$ points for the Brillouin zone. The convergence tolerance parameters were as follows: energy $5 \cdot 10^{-6}$ eV, force 0.01 eV \AA^{-1} ; stress 0.02 GPa; displacement 0.05 \AA . The total energy convergence criterion was assumed to be fulfilled when the self-consistent field tolerance reaches the value 10^{-7} eV per atom. The *ab initio* simulation of the features of electronic and spin subsystems in the framework of electron density functional theory (DFT) allows us to estimate the values of spin density (figure 7) in the vicinity of all species' sites present in the investigated system. The supercell of $3 \times 3 \times 1$ unit cells of FePS_3 single-crystal was used for modelling the proper concentration of Cu substitutional atoms. A pair of Cu was used to preserve the symmetry of the $\text{Cu}_{0.15}\text{Fe}_{0.85}\text{PS}_3$ lattice.

Components of the EFG tensor and asymmetry parameter η for Fe ions close to the experimental value for FePS_3 crystal ($\eta \approx 0.23$ – 0.28) were calculated for the system under study at $T = 0$ K (table 1).

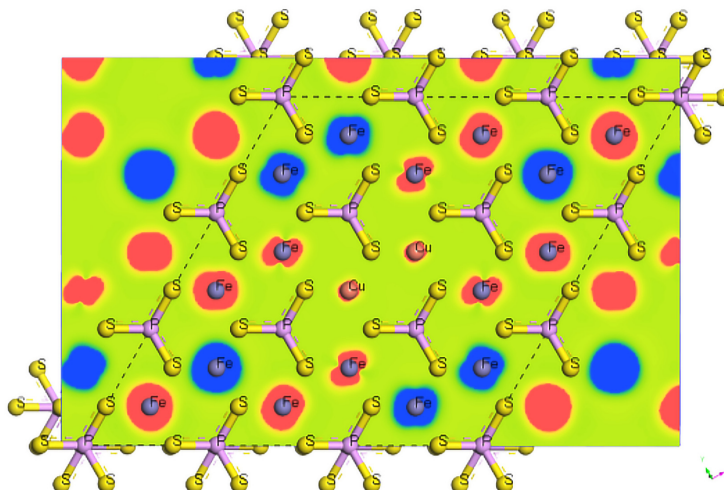


Figure 7. (Colour online) Spatial distribution of the calculated spin density of the $\text{Cu}_{0.15}\text{Fe}_{0.85}\text{PS}_3$ model at 0 K. Red and blue regions correspond to opposite spin orientations.

Table 1. Calculated averaged components of the EFG tensor and asymmetry parameter for $\text{Cu}_{0.15}\text{Fe}_{0.85}\text{PS}_3$ crystal.

Species	$\langle C_q \rangle$, MHz	$\langle \eta \rangle$
Cu	-3.1501	0.8797
Fe	11.2971	0.2911
P	32.7594	0.2774
S	-26.1410	0.0941

Furthermore, analysis of the Mulliken population shows that the main contribution to the ferromagnetic spin density is originated from $3d$ -copper and $3p$ -sulfur orbitals (see table 2).

Table 2. Decomposition of spin density (spin up – spin down) contributions over orbitals in $\text{Cu}_{0.15}\text{Fe}_{0.85}\text{PS}_3$ crystal. The largest contributions are typed in bold.

Species	$3d$	$3p$	$4f$	$4s$	Total
Cu	-0.248	-0.028	0.000	-0.002	-0.278
Fe	-0.087	0.030	0.010	-0.002	-0.049
P	-0.028	-0.030	0.000	0.000	-0.058
S	-0.072	-0.282	0.000	-0.016	-0.370
Total	-0.435	-0.310	0.010	-0.020	-0.755

The values of the valence charge transfer and the spin polarization were estimated for the $\text{Cu}_{0.15}\text{Fe}_{0.85}\text{PS}_3$ crystal (table 3). The presence of uncompensated spin ordering is found.

5. Discussions

In contrast to the expectation that Cu with spin $\frac{1}{2}$ will dilute the magnetic moments contributed by Fe with a larger spin, we found that 15% Cu doping partially keeps the effective fluctuating moment, although there is a long-range magnetic order partially distorted. This follows from the magnetic susceptibility

Table 3. The calculated values of the spin components of the valence charge and the spin polarization in $\text{Cu}_{0.15}\text{Fe}_{0.85}\text{PS}_3$ crystal.

Species	Q_{up}, e	Q_{dw}, e	Q, e	$\Sigma S, \hbar/2$
Cu	15.31 ± 0.00	15.45 ± 0.00	-3.53	-0.28
Fe	13.86 ± 1.36	13.86 ± 1.37	-27.51	-0.07
P	7.16 ± 0.03	7.16 ± 0.03	12.22	-0.07
S	7.82 ± 0.08	7.83 ± 0.07	18.82	-0.35

temperature dependence around transition from paramagnetic into antiferromagnetic phase — amplitude of the observed $\chi(T)$ anomaly is like the one observed in case of FePS_3 pure crystal [23]. At Fe by Cu partial substitution, the temperature of $\chi(T)$ maximum is lowered from 120 K in FePS_3 to 108 K in case of $\text{Cu}_{0.15}\text{Fe}_{0.85}\text{PS}_3$. The jump of $\chi(T)$ at ferromagnetic transition is smeared by Cu dilution.

In real crystal, the sulfur vacancies V_S presence can also effectively suppress the strong intralayer antiferromagnetic correlation, giving rise to a weak ferromagnetic ground state, which is observed on the $M(H)$ dependence below 10 K. The presence of V_S disrupts anion-mediated AFM interactions and may be responsible for the suppression of long-range AFM correlations. Herein, the competing ferromagnetic exchange interactions can dominate at low temperatures, creating a magnetically frustrated system. The exchange interactions between the V_S and metal ions, and with the local atomic distortion in the vicinity of defects, could also induce ferromagnetism.

A canting configuration and the resulting net moments along the easy axis can also be attributed to atomic substitution. All these signatures exhibit the complexity of magnetic structure for the 15% Cu substituted sample.

The susceptibilities of $\text{Cu}_{0.15}\text{Fe}_{1.85}\text{PS}_3$ can be considered as for configurationally averaged clusters sum of two terms: a randomly diluted antiferromagnet susceptibility, as in pure FePS_3 , and a Curie correction arising from local fluctuations of the uncompensated spins due to the finite size of the cluster. For $\text{Cu}_{0.15}\text{Fe}_{1.85}\text{PS}_3$ crystal, there is observed a weak paramagnetic contribution for small temperatures (figure 4), because many of the spins no longer belong to the infinite cluster. The uncompensated moments in the diluted 2D AFM can give rise to a Curie contribution into the magnetic susceptibility, and the presence of field dependence of the magnetization suggests that they interact ferromagnetically to give a spontaneous magnetization below 10 K.

6. Conclusions

According to the presented experimental data on Mössbauer spectroscopy and direct magnetic moment temperature and field dependencies measurements, it can be stated that the $\text{Cu}_{0.15}\text{Fe}_{0.85}\text{PS}_3$ single-crystal undergoes a magnetic phase transition at the region of 102–108 K. A weak ferromagnetic moment at the low-temperature region ($T = 10$ K) was observed in the $H \perp$ plane direction. This correlates with *ab initio* calculated non-zero spin polarization of the considered material. Furthermore, the calculated values of the electric field gradient components and estimations of the total magnetic moment of the unit cell (0.764 $\hbar/2$ corresponds to 8.543 emu/mol) are in reasonable agreement with the measured experimental quantities of ~ 9 emu/mol.

The present studies of $\text{Cu}_{0.15}\text{Fe}_{0.85}\text{PS}_3$ magnetic properties show that the uncompensated moments in the diluted 2D AFM can give rise to a Curie contribution, and the observed field dependence of the magnetization suggests that they do interact ferromagnetically to give a spontaneous magnetization at low temperatures. The relation of the magnetic ordering with structural change at antiferromagnetic phase transition can also be important and must be investigated further on.

It is worth to note that the flattening of magnetic susceptibility at low temperature was also observed in rare-earth containing compounds caused by Kondo effect [33]. In the case of the studied $\text{Cu}_{0.15}\text{Fe}_{0.85}\text{PS}_3$ crystal, the system seems not to be such a strongly correlated material as rare earth materials but, of course, the proper investigation of the low temperature dependence of resistivity is needed.

References

1. Chu J., Wang Y., Wang X., Hu K., Rao G., Gong C., Wu C., Hong H., Wang X., Liu K., Gao C., Xiong J., *Adv. Mater.*, 2020, **33**, 2004469, doi:10.1002/adma.202004469.
2. Hu T., Kan E., *WIREs Comput. Mol. Sci.*, 2019, **9**, e1409, doi:10.1002/wcms.1409.
3. Liu Z., Deng L., Peng B., *Nano Res.*, 2021, **14**, 1802–1813, doi:10.1007/s12274-020-2860-3.
4. Gong C., Kim E. M., Wang Y., Lee G., Zhang X., *Nat. Commun.*, 2019, **10**, 2657, doi:10.1038/s41467-019-10693-0.
5. Wang F., Shifa T. A., Yu P., He P., Liu Y., Wang F., Wang Z., Zhan X., Lou X., Xia F., He J., *Adv. Funct. Mater.*, 2018, **28**, 1802151, doi:10.1002/adfm.201802151.
6. Gong C., Li L., Li Z., Ji H., Stern A., Xia Y., Cao T., Bao W., Wang C., Wang Y., Qiu Z. Q., Cava R. J., Louie S. G., Xia J., Zhang X., *Nature*, 2017, **546**, 265–269, doi:10.1038/nature22060.
7. Belianinov A., He Q., Dziaugys A., Maksymovych P., Eliseev E., Borisevich A., Morozovska A., Banyas J., Vysochanskii Yu., Kalinin S. V., *Nano Lett.*, 2015, **15**, 3808–3814, doi:10.1021/acs.nanolett.5b00491.
8. Liu F., You L., Seyler K. L., Li X., Yu P., Lin J., Wang X., Zhou J., Wang H., He H., Pantelides S. T., Zhou W., Sharma P., Xu X., Ajayan P. M., Wang J., Liu Z., *Nat. Commun.*, 2016, **7**, 12357, doi:10.1038/ncomms12357.
9. Qi J., Wang H., Chen X., Qian X., *Appl. Phys. Lett.*, 2018, **113**, 043102, doi:10.1063/1.5038037.
10. Osada M., Sasaki T., *APL Mater.*, 2019, **7**, 120902, doi:10.1063/1.5129447.
11. Lai Y., Song Z., Wan Y., Xue M., Wang C., Ye Y., Dai L., Zhang Z., Yang W., Dua H., Yangace J., *Nanoscale*, 2019, **11**, 5163–5170, doi:10.1039/C9NR00738E.
12. Dziaugys A., Shvartsman V. V., Macutkevicius J., Banyas J., Vysochanskii Yu., Kleemann W., *Phys. Rev. B*, 2012, **85**, 134105, doi:10.1103/PhysRevB.85.134105.
13. Kleemann W., Shvartsman V. V., Borisov P., Banyas J., Vysochanskii Yu. M., *Phys. Rev. B*, 2011, **84**, 094411, doi:10.1103/PhysRevB.84.094411.
14. Olsen T., *J. Phys. D: Appl. Phys.*, 2021, **54**, 314001, doi:10.1088/1361-6463/ac000e.
15. Wildes A. R., Zhitomirsky M. E., Ziman T., Lançon D., Walker H. C., *J. Phys. D: Appl. Phys.*, 2020, **127**, 223903, doi:10.1063/5.0009114.
16. Sakai H., Yamazaki T., Machida N., Shigematsu T., Nasu S., *Mol. Cryst. Liq. Cryst. Sci. Technol., Sect. A*, 2000, **341**, 105–110, doi:10.1080/10587250008026125.
17. Chandrasekharan N., Vasudevan S., *Phys. Rev. B*, 1996, **54**, 14903, doi:10.1103/PhysRevB.54.14903.
18. Mulders A. M., Klaasse J. C. P., Goossens D. J., Chadwick J., Hicks T. J., *J. Phys.: Condens. Matter*, 2002, **14**, 8697, doi:10.1088/0953-8984/14/37/306.
19. Masubuchi T., Hoya H., Watanabe T., Takahashi Y., Ban S., Ohkubo N., Takase K., Takano Y., *J. Alloys Compd.*, 2008, **460**, 668–674, doi:10.1016/j.jallcom.2007.06.063.
20. Bhutani A., Zuo J. L., McAuliffe R. D., dela Cruz C. R., Shoemaker D. P., *Phys. Rev. Mater.*, 2020, **4**, 034411, doi:10.1103/PhysRevMaterials.4.034411.
21. Dziaugys A., Macutkevicius J., Svirskas S., Juskenas R., Wencka M., Banyas J., Motria S. F., Vysochanskii Yu., *J. Alloys Compd.*, 2015, **650**, 386–392, doi:10.1016/j.jallcom.2015.07.261.
22. WissEl, Data Evaluation Software — WissEl, Wissenschaftliche Elektronik GmbH, [Online; accessed 10-Jul-2022], URL http://www.wissel-gmbh.de/index.php?option=com_content&task=view&id=55&Itemid=116.
23. Jernberg P., Bjarman S., Wäppling R., *J. Magn. Magn. Mater.*, 1984, **46**, 178–190, doi:10.1016/0304-8853(84)90355-X.
24. Chen Y. L., Yang D. P., *Mössbauer Effect in Lattice Dynamics: Experimental Techniques and Applications*, Wiley-VCH Verlag GmbH & Co. KGaA, Weinheim, 2007.
25. Rule K. C., Cashion J. D., Mulders A. M., Hicks T. J., *Hyperfine Interact.*, 2002, **141**, 219–222, doi:10.1023/A:1021286910897.
26. Giannozzi P., Baroni S., Bonini N., Calandra M., Car R., Cavazzoni C., Ceresoli D., Chiarotti G. L., Cococcioni M., Dabo I. et al., *J. Phys.: Condens. Matter*, 2009, **21**, 395502, doi:10.1088/0953-8984/21/39/395502.
27. Perdew J. P., Burke K., Ernzerhof M., *Phys. Rev. Lett.*, 1997, **78**, 1396, doi:10.1103/PhysRevLett.78.1396.
28. Ceperley D. M., Alder B. J., *Phys. Rev. Lett.*, 1980, **45**, 566, doi:10.1103/PhysRevLett.45.566.
29. Perdew J. P., Zunger A., *Phys. Rev. B*, 1981, **23**, 5048, doi:10.1103/PhysRevB.23.5048.
30. Grimme S., *J. Comput. Chem.*, 2006, **27**, 1787–1799, doi:10.1002/jcc.20495.
31. Vanderbilt D., *Phys. Rev. B*, 1990, **41**, 7892, doi:10.1103/PhysRevB.41.7892.
32. Monkhorst H. J., Pack J. D., *Phys. Rev. B*, 1976, **13**, 5188, doi:10.1103/PhysRevB.13.5188.
33. Menth A., Buehler E., Geballe T. H., *Phys. Rev. Lett.*, 1969, **22**, 295, doi:10.1103/PhysRevLett.22.295.

Антиферромагнітний фазовий перехід в шаруватому напівпровіднику $\text{Cu}_{0.15}\text{Fe}_{0.85}\text{PS}_3$: експеримент та DFT моделювання

В. Пащенко¹, О. Блудов¹, Д. Балтрунас², К. Мазейка², С. Мотря³, К. Глухов³, Ю. Височанський³

¹ Інститут фізики і техніки низьких температур ім. Б. Веркіна НАН України, просп. Науки 47, 61103, Харків, Україна

² Відділ ядерних досліджень Центру фізичних наук та технології, просп. Саваноріу 231, LT-02300, Вільнюс, Литва

³ Інститут фізики і хімії твердого тіла, Ужгородський національний університет, вул. Волошина 54, 88000, Ужгород, Україна

Представлені експериментальні дослідження парамагнітно-антиферромагнітного фазового переходу методом мессбауерівської спектроскопії та вимірювання температурних і польових залежностей магнітної сприйнятливості в шаруватому кристалі $\text{Cu}_{0.15}\text{Fe}_{0.85}\text{PS}_3$. Особлива поведінка польової залежності намагніченості в області низьких температур свідчить про слабкий феромагнетизм досліджуваного матеріалу. За допомогою *ab initio* моделювання електронної та спінової підсистем, в рамках теорії функціоналу електронної густини, проаналізовано особливості спінового впорядкування при низькій температурі, а також зміни міжатомних взаємодій поблизу атомів заміщення Cu. Розраховані компоненти тензора градієнта електричного поля та параметра асиметрії для іонів Fe близькі до значень знайдених з мессбауерівських спектрів. Малікенівські заселеності показують, що основний внесок у феромагнітну спінову густину вносять $3d$ орбіталі міді та $3p$ сірки. Розрахунковий загальний магнітний момент елементарної комірки (8.543 етм/мол) цілком узгоджується з виміряним експериментальним значенням ~ 9 етм/мол.

Ключові слова: метал-фосфорні трихалькогеніди, магнітне впорядкування, мессбауерівська спектроскопія, фазові переходи, теорія функціоналу електронної густини
